Vortex model of plane Poiseuille flow of non-Newtonian fluid

Victor L. Mironov and Sergey V. Mironov

[a]Institute for Physics of Microstructures, Russian Academy of Sciences, GSP-105, Nizhny Novgorod, 603950, Russia

Abstract

We present a description of plane Poiseuille flow of non-Newtonian time-independent fluid based on symmetric equations, which take into account both the longitudinal motion and rotation of the vortex tubes. This model has analytical solution in the form of the two-parametric velocity distribution, which is in good agreement with velocimetry data in microchannels. The advantage of this approach is that, in contrast to the Ostwald-de Waele power law, it provides a more accurate approximation of experimental velocity profiles for different Reynolds numbers by model profiles corresponding to the same viscosity parameter. We believe that this simple model can be useful for making adequate estimates for the parameters of non-Newtonian time-independent fluids in engineering hydrodynamics.

Keywords: Time-independent fluid, vortex tubes rotation, Ostwald-de Waele power law, shear viscosity

1. Introduction

Non-Newtonian fluids are characterized by a nonlinear shear stress - shear rate dependence [1]. Conventionally, they can be divided into three main categories: time-independent, time-dependent and viscoelastic fluids, which are described by different rheological models [1]-[6]. In particular, the rheological behavior of time-independent fluids is often described by so-called Ostwald-de Waele's (OW) power law. In this model, the relationship between effective (apparent) viscosity (ν_e) and shear rate is represented as a function of the power law index (n) and the flow consistency (m) [2]. For a plane (x, y) flow with velocity directed along the X axis, the OW law is written in the

following form

$$\nu_e = m \left(\frac{\partial u}{\partial y} \right)^{n-1} , \tag{1}$$

where u is the x-component of the velocity. Most real time-independent non-Newtonian fluids are shear-thinning fluids and in this case $0 < n < 1$. This simple model is widely used to approximate experimental data in scientific and engineering research.

Experimentally, the rheological properties of non-Newtonian fluids are established using rheometers [7],[8] and by measuring the Poiseuille flow velocity distribution in the middle section of microchannels [9]-[17]. In case of plane Poiseuille flow the power law (1) gives the following simple relation for the normalized velocity [9],[10]

$$\frac{u}{u_{\max}} = 1 - \left(\frac{y}{h} \right)^{\frac{n+1}{n}} , \tag{2}$$

where $2h$ is the channel width. Expression (2) allows one to classify various fluids in accordance with the index n. However, the experimental studies [9] show that the normalized velocity profiles of real fluids are determined not only by the index n, but also significantly depend on the Reynolds number (Re). This leads to the fact that power law indexes measured from the velocity profiles for the same fluid depend on the average flow velocity and differ from the values measured using a rheometer [9].

In current paper, we propose an alternative model for describing the rheological behavior of a non-Newtonian fluid based on a system of equations for a vortex flow [18],[19]. These equations describe both the longitudinal motion of the fluid and take into account the rotation of vortex tubes in a shear flow. Within the framework of this model, we obtained an analytical expression for the velocity profile of a plane Poiseuille flow. It is shown that the velocity profile is determined by two parameters, which makes it possible to fit model and experimental velocity profiles for different Reynolds numbers using *the same viscosity value*. All calculated velocity distributions are in good agreement with the experimental data.

2. Vortex model of plane flow

A vortex flow of isentropic incompressible viscous fluid can be described by the following symmetric system of equations [18]:

$$\frac{1}{c}\left(\frac{\partial}{\partial t} + (\mathbf{v} \cdot \nabla) - \nu\Delta\right)\mathbf{v} + \nabla \times \mathbf{w} + \frac{1}{c\rho}\nabla p = 0,$$

$$\frac{1}{c}\left(\frac{\partial}{\partial t} + (\mathbf{v} \cdot \nabla) - \nu\Delta\right)\mathbf{w} - \nabla \times \mathbf{v} = 0, \tag{3}$$

$$\nabla \cdot \mathbf{v} = 0,$$

$$\nabla \cdot \mathbf{w} = 0.$$

Here c is a speed of sound $(c^2 = (\partial p/\partial\rho)_s)$, $\mathbf{v}$ is a local velocity, ν is a kinematic viscosity, ρ is a fluid density, p is a pressure. The vector $\mathbf{w}$ characterizes the rotation of the vortex tube around its axis

$$\mathbf{w} = 2c\,\boldsymbol{\theta},$$

$$\boldsymbol{\omega} = \frac{d\boldsymbol{\theta}}{dt}, \tag{4}$$

where $\boldsymbol{\theta}$ is the angular vector of rotation and $\boldsymbol{\omega}$ is the angular velocity of the vortex tube rotation.

Let us consider the steady-state plane flow parallel to the plane xy with the velocity directed along the X axis. In this case the velocity $\mathbf{v}$ has only x component and depends only on the y coordinate $\mathrm{v}_x = \mathrm{v} = \mathrm{v}(y, t)$. Similarly, in plane flow the vector of rotation angle $\mathbf{w}$ has only z component and depends only on y coordinate $\mathrm{w}_z = \mathrm{w} = \mathrm{w}(y, t)$. Also we assume that $\frac{1}{c\rho}\frac{\partial p}{\partial x} = -g = const$. Then in the projection on the X and Z axes, the system of equations (3) for the plane flow takes the following form

$$\frac{1}{c}\frac{\partial \mathrm{v}}{\partial t} - \lambda\frac{\partial^2 \mathrm{v}}{\partial y^2} + \frac{\partial \mathrm{w}}{\partial y} - g = 0,$$

$$\frac{1}{c}\frac{\partial \mathrm{w}}{\partial t} - \lambda\frac{\partial^2 \mathrm{w}}{\partial y^2} + \frac{\partial \mathrm{v}}{\partial y} = 0. \tag{5}$$

Here we introduced the characteristic length $\lambda = \nu/c$.

3

To describe a steady-state flow, we introduce the time-averaged values. For any value $a(y, t)$, averaging over time is carried out as follows:

$$\overline{a(y)} = \lim_{T \to \infty} \frac{1}{2T} \int\limits_{-T}^{T} a(y, t) dt. \tag{6}$$

Also we will consider the uniform tubes rotation with angular velocity $\omega(y)$ and different phases $\varphi(y)$

$$\mathrm{w}(y, t) = 2c\omega(y)t + \varphi(y). \tag{7}$$

Then the for steady-state flow we have

$$\overline{\frac{\partial \mathrm{v}}{\partial t}} = 0,$$
$$\overline{\mathrm{w}(y)} = \varphi(y), \tag{8}$$
$$\overline{\frac{\partial \mathrm{w}}{\partial t}} = \omega(y).$$

Taking into account (6)-(8) we obtain the following time-averaged equations:

$$-\lambda \frac{\partial^2 \bar{\mathrm{v}}}{\partial y^2} + \frac{\partial \bar{\mathrm{w}}}{\partial y} - g = 0,$$
$$-\lambda \frac{\partial^2 \bar{\mathrm{w}}}{\partial y^2} + \frac{\partial \bar{\mathrm{v}}}{\partial y} + 2\omega(y) = 0. \tag{9}$$

3. Plane Poiseuille flow

In case of plane Poiseuille flow in a channel with fixed walls (Fig. 1), the fluid moves under the action of the pressure gradient.

Let us consider fully developed steady-state Poiseuille flow. We assume that angular speed of vortex tubes rotation is the linear function of y coordinate $\omega(y) = \kappa y$. In this case the equations (9) take the following form:

$$-\lambda \frac{\partial^2 \bar{\mathrm{v}}}{\partial y^2} + \frac{\partial \bar{\mathrm{w}}}{\partial y} - g = 0,$$
$$-\lambda \frac{\partial^2 \bar{\mathrm{w}}}{\partial y^2} + \frac{\partial \bar{\mathrm{v}}}{\partial y} + 2\kappa y = 0. \tag{10}$$
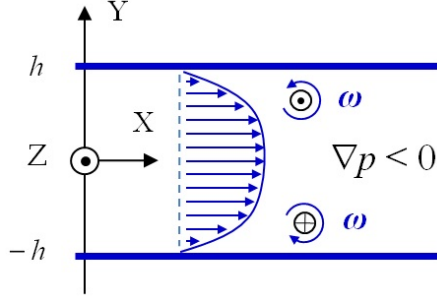
4

Figure 1: Sketch of plane Poiseuille flow in a channel between two infinite plates under the gradient of pressure.
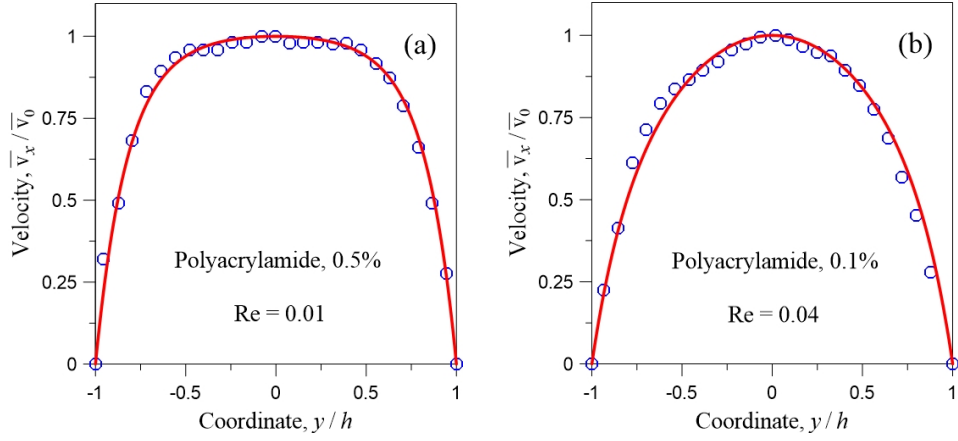

Figure 2: Normalized velocity profiles for Polyacrylamide solution with different concentration and different Reynolds numbers. Experimental data are shown with circles [10]. The results of fitting according to formula (12) are shown by a solid red line. Fitting parameters (a) $\lambda/h = 0.172$, $\sigma = 0.98$; (b) $\lambda/h = 0.17$, $\sigma = 0.7$.

We consider the boundary conditions corresponding to the complete adhesion of the fluid to the plate surface

$$
\begin{aligned}
\bar{v}(h) &= \bar{v}(-h) = 0, \\
\varphi(h) &= \varphi(-h) = 0.
\end{aligned}
\tag{11}
$$

The solutions of the system (10) are

$$
\bar{v} = \sigma g h \frac{\cosh(h/\lambda) - \cosh(y/\lambda)}{\sinh(h/\lambda)} + g h^2 \frac{(1-\sigma)}{2\lambda}\left(1 - \frac{y^2}{h^2}\right),
\tag{12}
$$

$$\varphi = -\sigma g h \left(\frac{\sinh(y/\lambda)}{\sinh(h/\lambda)} - \frac{y}{h} \right), \tag{13}$$

where σ is a certain parameter connected with pressure gradient and transverse gradient of angular velocity

$$\sigma = 1 - \frac{2\lambda\kappa}{g}. \tag{14}$$

For comparison with experiment, we normalized the velocity distribution (12) to the maximum velocity $\bar{v}_0$ ($\bar{v}_0$ is the velocity at $y = 0$). As an example, Fig. 2 demonstrates the fitting of the experimental velocity profiles for Polyacrylamide solution with different concentration and different Reynolds numbers [10] by the normalized distribution (12). As one can see, there is good agreement between the simulated curves and experimental data.

4. Discussion

In distribution (12) the parameter σ describes the relationship between the parabolic and hyperbolic velocity profiles.

For $\sigma = 0$ the velocity distribution has the purely parabolic profile

$$\bar{v} = \frac{gh^2}{2\lambda} \left(1 - \frac{y^2}{h^2} \right). \tag{15}$$

On the other hand, when $\sigma = 1$ we have the purely hyperbolic profile:

$$\bar{v} = gh \frac{\cosh(h/\lambda) - \cosh(y/\lambda)}{\sinh(h/\lambda)}. \tag{16}$$

The normalized distribution (16) is

$$\frac{\bar{v}}{\bar{v}_0} = \frac{\cosh(h/\lambda) - \cosh(y/\lambda)}{\cosh(h/\lambda) - 1}, \tag{17}$$

where $\bar{v}_0$ is the velocity in the maximum at $y = 0$. This profile is very close to the profile described by OW power law (2). For comparison, Fig. 3 demonstrates several OW profiles (2) for different indexes n and the profiles (17) for corresponding parameters λ/h. Additionally, the correspondence between the index n and parameter λ/h is represented graphically in Fig. 4. One can see that there is an unambiguous correspondence between the parameter λ/h and the index n.
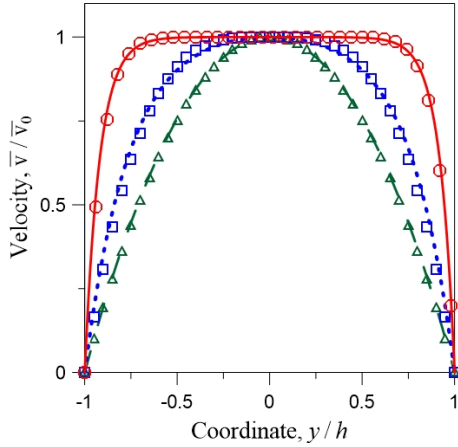
6

Figure 3: The velocity profiles of Poiseuille flow described by distributions (2) and (17). Symbols and lines correspond to: triangles $n = 1$, dashed green line $\lambda/h = 1$; squares $n = 0.4$, dotted blue line $\lambda/h = 0.24$; circles $n = 0.1$, solid red line $\lambda/h = 0.08$.
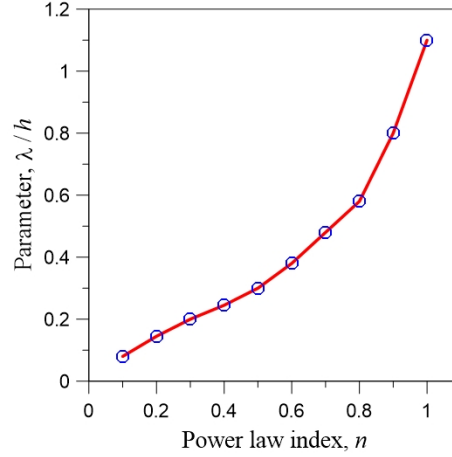
Figure 4: Diagram of the correspondence between power law index n and parameter λ/h.

The OW law (2) describes the stationary velocity profiles of a non-Newtonian fluid quite well. However, in case of approximating the velocity profiles for flows with different Re, the different indexes n are obtained [9]. In this sense, the index n characterizes not so much the viscous properties of the fluid itself, but rather the dynamic properties of the flow. On the contrary, the two-parametric model of vortex flow (12) allows one to approximate the velocity profiles at different Re with the same parameter λ/h, which is determined by the kinematic viscosity of the fluid. Fig. 5 shows several model velocity profiles corresponding to the same parameter $\lambda/h = 0.08$ but different values of the parameter σ. As one can see, the parameter σ varies the velocity profiles over a wide range that can be used to match the modeling results and experimental data. As an example, Fig. 6 demonstrates the results of fitting experimental profiles [9] for flows of Polyacrylamide solution (0.4%) with different Re. One can see good agreement between the calculated and experimental profiles for the same values of parameter λ/h, but for different values of parameter σ.
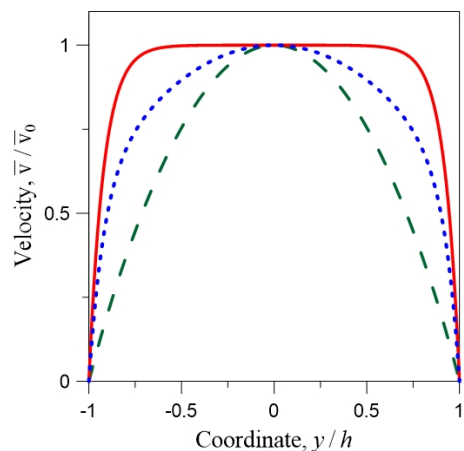
7

Figure 5: Velocity profiles (12) in dependence on parameter σ. Solid red line $\sigma = 1$; dotted blue line $\sigma = 0.8$; dashed green line $\sigma = 0.1$.
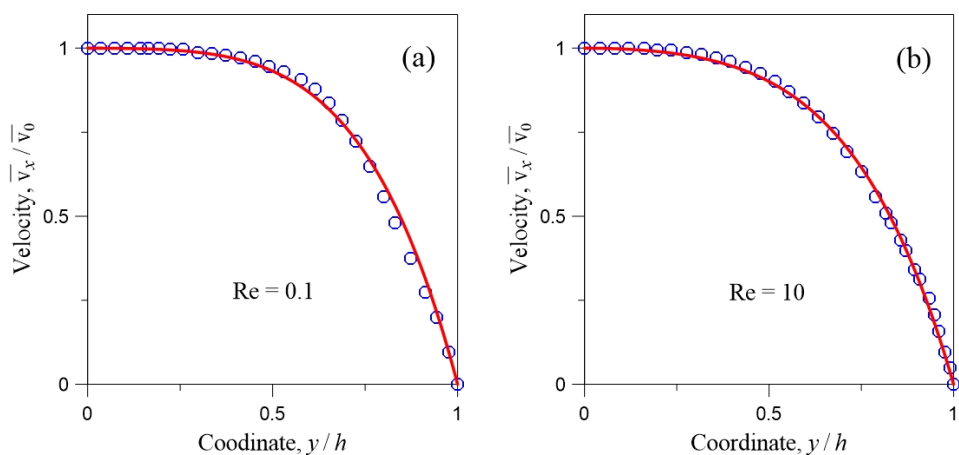

Figure 6: Velocity profiles for the flow of Polyacrylamide solution (0.4%) with different Re. Experimental data [9] are shown by circles, the results of fitting according to formula (12) are shown by solid lines. (a) $n = 0.34$, $\lambda/h = 0.45$, $\sigma = 1.85$. (b) $n = 0.4$, $\lambda/h = 0.45$, $\sigma = 1.69$.

5. Concluding remarks

Thus, we have considered the model of time-independent non-Newtonian fluid based on equations that take into account the rotation of vortex tubes in the shear flow. It is shown that the obtained two-parametric velocity

8

distribution well describes the experimentally measured velocity profiles. The advantage of this model is that the agreement with experimental data is achieved at the fixed parameter λ/h (determined by the viscosity of the fluid) by fitting the parameter σ, which actually takes into account the effects associated with changes in Reynolds numbers. In addition, this model can be simply generalized to the case of purely shear Couette flow and combined Couette-Poiseuille flow.

Acknowledgement

References

[1] F. Irgens, "*Rheology and non-Newtonian fluids*", Springer, (2013).

[2] R.P. Chhabra, "Non-Newtonian Fluids: An Introduction", In: "*Rheology of Complex Fluids*" (eds J. Krishnan, A. Deshpande, P. Kumar), Springer, New York, p. 3-34 (2010).

[3] M. Zatloukal, A simple phenomenological non-Newtonian fluid model, Journal of Non-Newtonian Fluid Mechanics, **165**, 592-595 (2010).

[4] L. Wang, J. Mi, X. Meng, Z. Guo, A localized mass-conserving lattice Boltzmann approach for non-Newtonian fluid flows, Communications in Computational Physics, **17**(4), 908 – 924 (2015).

[5] D. Yao, A non-Newtonian fluid model with an objective vorticity, Journal of Non-Newtonian Fluid Mechanics, **218**, 99-105 (2015).

[6] R.J. Poole, Inelastic and flow-type parameter models for non-Newtonian fluids, Journal of Non-Newtonian Fluid Mechanics, **320**, 105106 (2023).

[7] C.W. Macosko, "*Rheology: principles, measurements and applications*", Viley-VCH Publishers, New York, (1994).

[8] Y.Y. Hou, H.O. Kassim, Instrument techniques for rheometry, Review of Scientific Instruments, **76**, 101101 (2005).

[9] S. Ansari, M. Rashid, P.R. Waghmare, D. S. Nobes, Measurement of the flow behavior index of Newtonian and shear-thinning fluids via analysis of the flow velocity characteristics in a mini-channel, SN Applied Sciences, **2**, 1787 (2020).

[10] T. Fu, O. Carrier, D. Funfschilling, Y. Ma, H.Z. Li, Newtonian and Non-Newtonian flows in microchannels: inline rheological characterization, Chemical Engineering and Technology, **39**(5), 987–992 (2016).

[11] C. Completo, V. Geraldes, V. Semiao, Micro-PIV characterization of laminar developed flows of Newtonian and non-Newtonian fluids in a slit channel, Engineering Mechanics, **19**(1), 3–13 (2012).

[12] C. Completo, V. Geraldes, V. Semiao, Rheological and dynamical characterization of blood analogue flows in a slit, International Journal of Heat and Fluid Flow, **46**(1), 17–28 (2014).

[13] S. Devasenathipathy, J.G. Santiago, S.T. Wereley, C.D. Meinhart, K. Takehara, Particle imaging techniques for microfabricated fluidic systems, Experiments in Fluids, **34**, 504–514 (2003).

[14] G. Degré, P. Joseph, P. Tabeling, S. Lerouge, M.l Cloitre, A. Ajdari, Rheology of complex fluids by particle image velocimetry in microchannels, Applied Physics Letters, **89**, 024104 (2006).

[15] C.D. Meinhart, S.T. Wereley, J.G. Santiago, PIV measurements of a microchannel flow, Experiments in Fluids, **27**(5), 414–419 (1999).

[16] G. Silva, N. Leal, V. Semiao, Micro-PIV and CFD characterization of flows in a microchannel: Velocity profiles, surface roughness and Poiseuille numbers, International Journal of Heat and Fluid Flow, **29**, 1211–1220 (2008).

[17] N. Erkan, K. Shinohara, S. Someya, K. Okamoto, Three-component velocity measurement in microscale flows using time-resolved PIV, Measurement Science and Technology, **19**(5), 057003 (2008).

[18] V.L. Mironov, S.V. Mironov, Generalized sedeonic equations of hydrodynamics, European Physical Journal Plus, **135**(9), 708 (2020).

[19] V.L. Mironov, S.V. Mironov, Vortex model of plane Couette flow, Fluids, **8**(6), 165 (2023).